Control strategy comparison of the 8/6 switched reluctance motor in several inverter topologies

Ronaldo Martua, Alam Raihan Emir, Michael Suhendra, Denri Yesayevtta, Arwindra Rizqiawan, Jihad Furqani

School of Electrical and Informatics, Institut Teknologi Bandung, Bandung, Indonesia

Article Info

ABSTRACT

This paper proposes a control strategy for switched reluctance motors (SRMs) using the asymmetric half-bridge (AHB), shared switch, and Miller converter based on MATLAB/Simulink and TMS320F28379D. The control strategy implemented in this study involves the application of proportional-integral (PI) speed control with a pulse width modulation (PWM) switching method for each topology. By employing this control strategy, the system aims to regulate the speed of the motor and achieve the desired performance while ensuring efficient power utilization. The PI controller is utilized to adjust the motor's speed based on the error between the desired and actual speeds, enabling precise control. Additionally, the PWM switching method is employed to modulate the motor voltage, allowing for smooth and continuous speed adjustments. A thorough method for maximizing each topology's performance and raising the overall system efficiency is provided by this combination of control techniques. The detailed analysis and operation of each converter are presented in this paper. Simulation and experiment results show that AHB and shared switch have better performance than Miller. But the Miller converter needs the least number of switching components. Although the performance of the shared switch is equal to that of AHB, uses of this topology are limited to SRM with an even number of phases.

Corresponding Author:

Ronaldo Martua
School of Electrical and Informatics, Institut Teknologi Bandung
Bandung, Indonesia
Email: ronaldomartua@gmail.com

1. INTRODUCTION

A switched reluctance motor (SRM) is an electric motor that operates based on the principle of variable reluctance. SRMs have a relatively simple mechanical structure compared to other motor types, reducing manufacturing complexity and cost [1]-[3]. Unlike traditional electric motors, SRMs do not have a permanent magnet in the rotor. Instead, the rotor is typically a simple piece of ferromagnetic material with salient poles. The absence of permanent magnets in the rotor enhances the robustness of SRMs, making them less susceptible to demagnetization and thermal issues. The stator, on the other hand, contains windings that are energized in a sequential manner to create a magnetic flux path, inducing motion in the rotor. SRMs exhibit good performance over a wide range of speeds and loads, making them versatile for various applications, and it can achieve high torque density [4]-[8]. However, it has significant torque ripple and acoustic noise as disadvantages, which can be a concern in applications where noise is a critical factor [9]-[13].

The operation of an SRM is characterized by the reluctance torque produced due to the alignment of the rotor and stator poles. Several crucial considerations must be taken into account, such as ensuring that all stator and rotor poles are not aligned simultaneously, as this would result in the absence of torque generation.

Consequently, the rotor and stator pole numbers cannot be equal. The motor phases are energized in a specific sequence, causing the rotor to move to the position of minimum reluctance. This circumstance also causes torque to be generated, which pushes the rotor into alignment [14]-[17].

There have been numerous SRM topologies that have been widely recognized thus far, including SRM 12/10, 8/6, 6/4, and others. This specific combination of numerical values effectively represents the total count of pole stator and rotor. The visual representation depicted in Figure 1(a) serves to illustrate SRM 8/6 topologies with four phase conditions. The region in orange clearly indicates the presence of eight stator poles, while the region in blue signifies the existence of six rotor poles. To establish a winding phase, the windings on B1 and B2 are meticulously connected in series. Consequently, a total of four-phase windings is ingeniously created, extending from A1-A2 all the way to D1-D2 [18]. SRM 8/6 has been extensively employed in numerous home appliances. This can be observed in Figure 1(b), which showcases the application of SRM 8/6 in some automatic cooking machines.

For driving the SRMs, it needs a converter. The converter that is utilized to drive SRM has certain prerequisites. These prerequisites include the converter having at least one switch that can independently conduct for each phase of the motor and possess the capability to excite the phase prior to entering the demagnetizing region [19]-[21]. Among the various converters available, the asymmetric half bridge (AHB) converter stands as the most widely accepted topology. This topology is known for its efficiency in fault-tolerant operations and its ability to control each phase independently. However, it is important to note that this topology does have its disadvantages, one of which is the presence of large switching components. Due to this drawback, the shared switch and Miller's topology can be considered as an optional alternative for driving SRMs. The shared switch topology, when compared to the AHB topology, requires fewer components but is limited to SRMs with an even number of phases. On the other hand, Miller's topology needs the fewest components.

The previous works provide a brief outlook about the performance of each topology for driving SRM, none of them comprehensively investigates the performance of each topology for SRM 8/6 with the same control strategy using PI control in voltage regulation mode with PWM. This paper will describe the small signal linearization method, the switching strategy, and model the simulation of SRMs with the control of firing angle and speed regulation using pulse width modulation (PWM) for AHB, Shared Switch, and Miller topology in the MATLAB/Simulink environment. Finally, the experimental tests, which employ the microcontroller TMS320F28379D with logic based on the MATLAB/Simulink environment, are conducted in order to validate the simulation result.
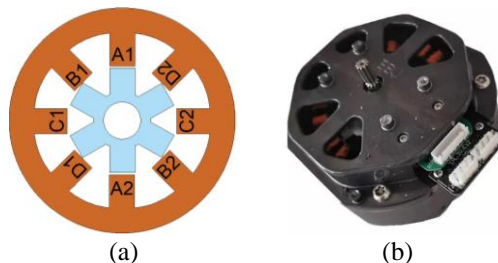

(a)　　　　　　(b)

Figure 1. Four phase-SRM 8/6: (a) topology and (b) actual unit for home appliances

2. CONTROL and SWITCHING STRATEGY

2.1 Control strategy: closed-loop control

The closed-loop control, which serves as the most elementary controller for the switched reluctance machine (SRM), is primarily utilized in speed control scenarios and does not demand optimal drive performance [22]. In its typical implementation scheme, as shown in Figure 2, the closed-loop control is comprised of several components, including a speed controller, a phase control method, and a block responsible for generating the switching signals. The speed controller, commonly employed in motor drives featuring different types of electrical machines, typically employs a linear proportional-integral (PI) controller. This controller receives the speed error and generates a reference voltage signal by determining the PWM duty cycle with the fixed frequency of the switching component.

The phase control component plays a crucial role in triggering each phase and determining how the reference voltage should be applied. To ensure the effectiveness of this phase control, it is imperative to have accurate rotor position measurements. To achieve this, there are various methods for determining the switching

angle. The most common strategy for the switching angle is described in Figure 3. The phase will magnetize when the phase inductance is at minimum condition (θ_{on}). The position of rotor and stator is unaligned in minimum phase inductance, and it will be off before it reaches maximum condition (θ_{off}). This strategy is used to prevent negative torque and achieve the needed current level, especially in high-speed applications [23]. The SRMs model in an electrical equation can be described as in (1):

$$V = i\,R_s + i\,\frac{\partial L(\theta)}{\partial \theta}\,\omega + L\,\frac{\partial i}{\partial t} \tag{1}$$

where V is the voltage, i is the current, R_s is the stator resistance, L phase inductance, θ is the rotor position, and ω is the rotor speed. The individual torque electric (T_e) equation can be described as in (2).

$$T_e = \frac{1}{2}\,i^2\,\frac{\partial L\,(\theta,i)}{\partial \theta} \tag{2}$$

The mechanical equation can be described as in (3):

$$T_e - T_l = B\,\omega + J\,\frac{\partial \omega}{\partial t} \tag{3}$$

where T_l is the torque load, B is friction coefficient, and J is SRM inertia. If we assume that the magnetic structure is non-saturated and the phase current is in a steady-state condition, so $L\,(\theta,i) \sim L(\theta)$. To effectively address the remaining non-linearities, it becomes imperative to undertake the process of linearizing the model. A widely employed technique in this regard is the linearization approach centered around an operation point, commonly referred to as small-signal linearization. The Linearized transfer function model of SRM is shown in Figure 4.
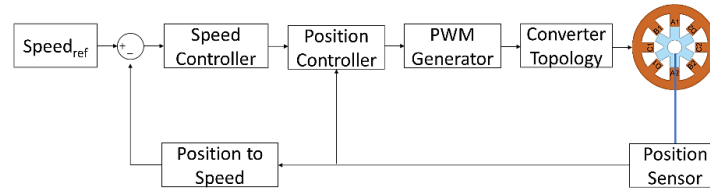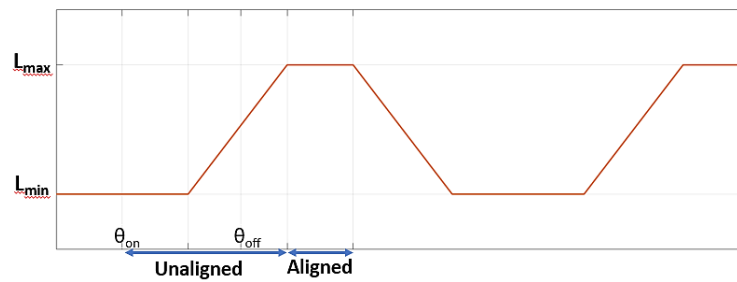

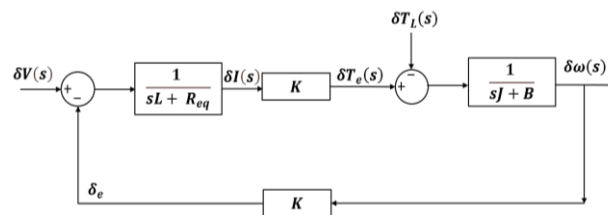Figure 2. Block diagram for speed control

Figure 3. SRMs phase inductance

Figure 4. Linearized transfer function of SRMs

2.2 Switching strategy: AHB

In order to drive the SRM 8/6, the AHB converter necessitates the utilization of eight switches and eight diodes. Figure 5 shows the topology employed by the AHB converter, which consists of two switches and two diodes for each phase. By employing this specific configuration, the AHB converter possesses the advantageous capability to independently regulate each phase without being hindered by the influence of other phases, despite the fact that the total number of switches surpasses that of other converter topologies [24].

The SRMs converter functions in three distinct modes: magnetizing, demagnetizing, and freewheeling [25]. These modes are described in Figures 6(a)-6(c). In these figures, the flow of current is represented by the red-colored circuit or components (active component), while the black-colored circuit or components represent the passive component. Figure 6(a) exemplifies the magnetizing mode of the AHB converter, wherein the excitation process for the A-phase winding is executed by activating switches S1 and S2.

The frequency switching is fixed to minimize electromagnetic interference. To achieve soft chopping through pulse width modulation (PWM), the freewheeling and magnetization modes are utilized by commutating the switches. Specifically, one switch is commutated while the other remains in the "ON" state for the entire duration. The freewheeling mode, as illustrated in Figure 6(b), involves reducing the voltage across the A-phase winding to zero, resulting in a gradual decrease in current.

Additionally, Figure 6(c) provides an explanation of the demagnetization mode of phase A and the subsequent magnetization mode of phase B. Prior to aligning the rotor and stator positions, which is indicated by maximum inductance, it is necessary to deactivate the stator current using the demagnetization mode (achieved by turning off switches S1 and S2 for phase A). Meanwhile, the next phase begins the magnetization mode. Figure 7 shows the switching signal of S1, S2, S5, and S6 in the AHB converter. S1 and S5 are controlled by rotor position, S2 and S6 are controlled by rotor position and PWM.
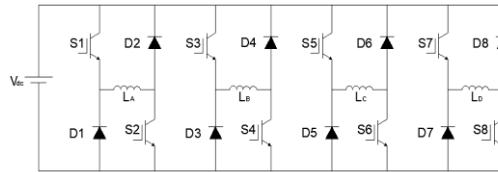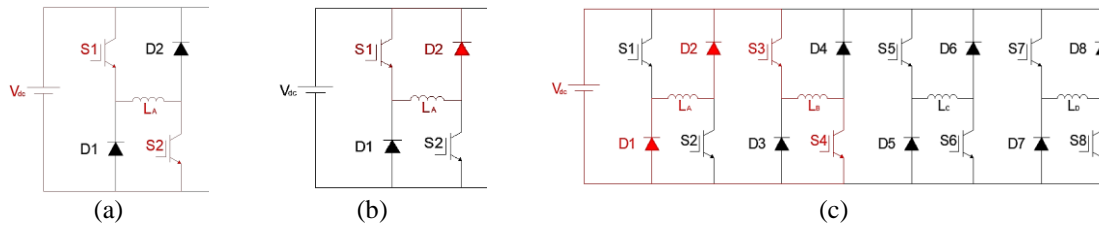

Figure 5. 4-Phase converter AHB

Figure 6. 4-Phase converter AHB working condition: (a) magnetization mode, (b) freewheeling mode, and (c) demagnetization mode of phase-A and continue to magnetize phase-B
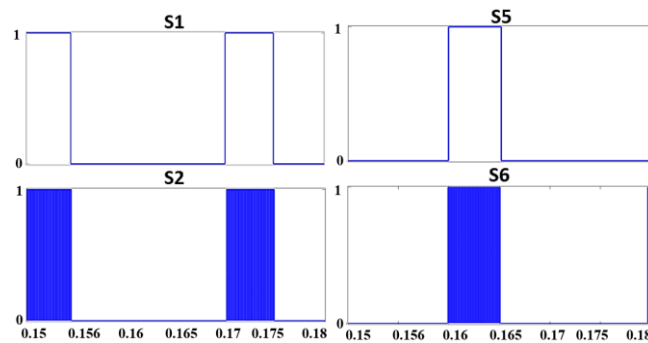

Figure 7. Switching signal for phase A and C through switch S1, S2, S5, S6 in AHB converter

2.3 Switching strategy: shared switch

Figure 8 presents the topology of a shared switch converter designed for SRM 8/6. This particular converter topology utilizes switches that are shared between non-adjacent phases. Specifically, switches S2 and S5 are shared between phases A-C and B-D, respectively. The advantage of this configuration is that it requires fewer switches per phase while still allowing for independent control of the phase current. To drive the SRM 8/6, this converter employs a total of 6 switches and 6 diodes. Consequently, the rating for switches S2 and S5 is higher than that of the phase switches S1, S2, S3, and S4. It is important to note that this topology is only applicable to SRMs with an even number of phases. The operation of each phase can be divided into three distinct modes, namely magnetization, freewheeling, and demagnetization, as depicted in Figure 9. Similar to Figure 6, the red-colored circuit or components represent the active components, while the black-colored ones are passive components.

To facilitate the explanation of the operation, let us begin by examining the waveform of this converter, which starts with the magnetization of phase A. This is achieved by turning ON switches S1 and S2, as shown in Figure 9(a). During magnetization in the shared switch, the voltage across the winding in phase A is equal to the input voltage Vdc, resulting in the generation of positive torque. Additionally, the inductance of phase A increases. Soft chopping by PWM is implemented by means of the freewheeling and magnetization modes, achieved by commutating one of the switches while maintaining the other switch in the "ON" state throughout the entire period, as depicted in Figure 9(b). In this mode, switch S1 is commutated, while switch S2 remains ON throughout the entire period.

When the positions of the rotor and stator are aligned, the activation of the demagnetization mode takes place. During this mode, the flow of current in the stator is halted, and phase B transitions into magnetization mode, as displayed in Figure 9(c). Switches S4 and S5 are employed for magnetization mode in phase B. The demagnetization mode of phase B is depicted in Figure 9(d), where switches S4 and S5 are deactivated, thereby causing phase C to enter magnetization mode. In phase C, switches S2 and S3 are utilized for magnetization mode. It is important to note that switch S3 carries the currents of phases A and C, while switch S5 carries the currents of phases B and D, as illustrated in Figure 9(e). This situation arises when phase C is in demagnetization mode and phase D transitions into demagnetization mode. Lastly, Figure 9(f) presents the functioning when phase D is in demagnetization mode and phase A commences magnetization mode. Figure 10 shows the switching signal of S2, S1, and S3 in shared switch converter when phases A and C are active. S2 is controlled by rotor position, S1 and S3 are controlled by rotor position and PWM.
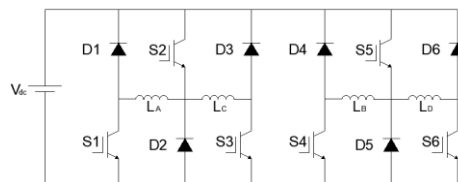

Figure 8. 4-Phase converter shared switch

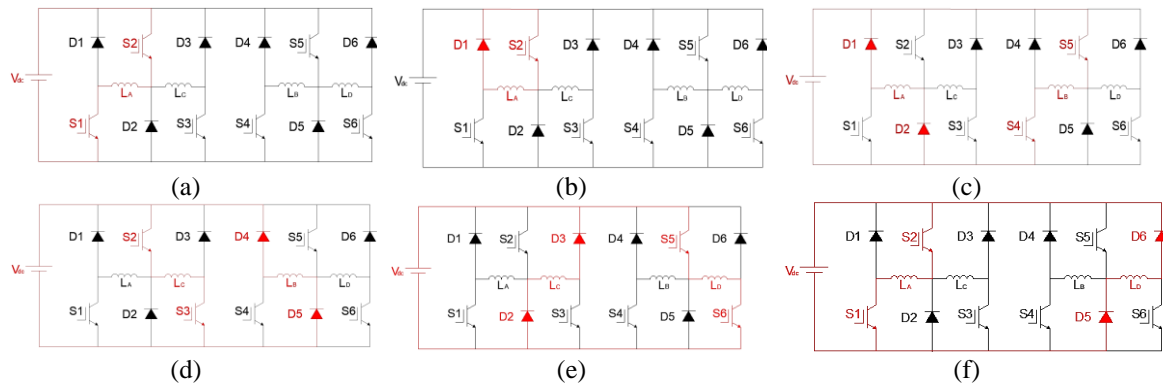| (a) | (b) | (c) |
| (d) | (e) | (f) |

Figure 9. 4-Phase converter shared switch working condition: (a) magnetization of phase a, (b) free-wheeling of phase A, (c) magnetization of phase B and demagnetization of phase A, (d) magnetization of phase C and demagnetization of phase B, (e) magnetization of phase D and demagnetization of phase C, and (f) magnetization of phase A and demagnetization of phase D
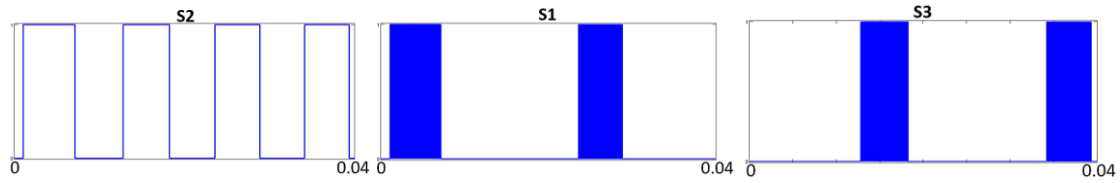
Figure 10. Switching signal for phase A and C through switch S2, S1, S3 in shared switch converter

2.4 Switching strategy: Miller

Figure 11 presents the topology of the Miller converter designed for the SRM 8/6. This particular topology offers notable advantages, namely the diminished count of power devices and the potential for independent phase control. Specifically, this topology shared S1 for phases A until D. However, it is not without its limitations. One such drawback is the inability to activate certain phases simultaneously.
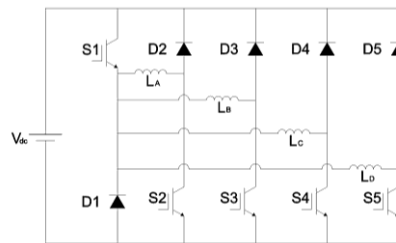
Figure 11. 4-Phase converter Miller

The magnetization of the Miller converter is shown in Figure 12(a) by switching ON the S1 and S2. Figure 12(b) shows the freewheeling condition, achieved by commutating switch S2 while maintaining the S1 in the "ON" state throughout the entire period. Before the rotor position is aligned with the stator, switches S1 and S2 should be OFF. It cannot simultaneously magnetize to phase-B since there is still residual current in phase A. It is necessary to switch OFF all the switches for several degrees to prevent the overlap situation, which leads to inefficient power consumption. The demagnetization of Miller topology is shown in Figure 12(c). After the current of phase A becomes zero, phase B can magnetize as shown in Figure 12(d). Figure 13 shows the switching signal of S1, S2, S3, S4 in the Miller converter when phases A, B, and C are active. S1 is controlled by rotor position, S2, S3, and S4 are controlled by rotor position and PWM.
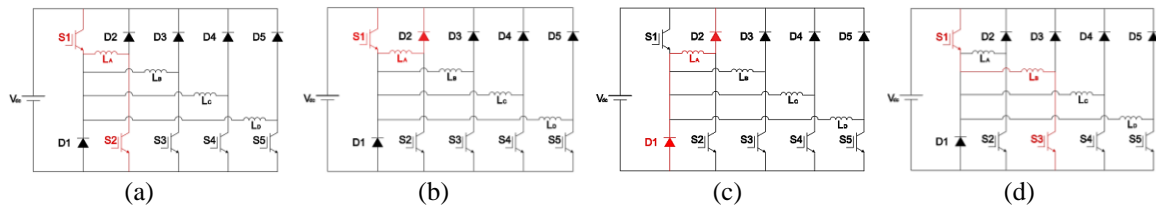

| (a) | (b) | (c) | (d) |

Figure 12. 4-Phase converter Miller working condition: (a) magnetization of phase A, (b) free-wheeling of phase A, (c) demagnetization of phase A, and (d) magnetization of phase B
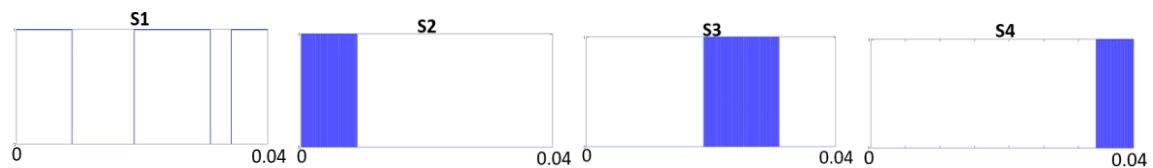

Figure 13. Switching signal for phase A, B, and C through switch S1, S2, S3, S4 in Miller converter

3.   SIMULATION

The control model and strategy are simulated using MATLAB/Simulink. Figure 14 shows the block diagram of the simulation in MATLAB. Switching logic will determine the condition of the switching components through position. The output of PI based speed control and switching logic will determine the switching components, which are controlled by position and PWM.

In order to accurately represent the motor load, a generic model of the 8/6 SRM was utilized. The simulation employed a set of parameters that are illustrated in Table 1. As you can see from the stator resistance until the current reference, these are the parameters of SRM 8/6. Those parameters are gotten from the actual SRM 8/6 that we used for the experiment. The load torque is 0.04 N.m. since the application of SRM 8/6 is for home appliances that have a small load torque. The other reason is because we only applied a small voltage to the converter for the experiment. Each converter is powered by 35 Vdc, and the switching frequency is 10 kHz. In this simulation, we try to maintain the speed of the SRM at 800 rpm using each topology. The simulation result determines parameters phase flux, phase current, torque electric, and speed for each converter topology.
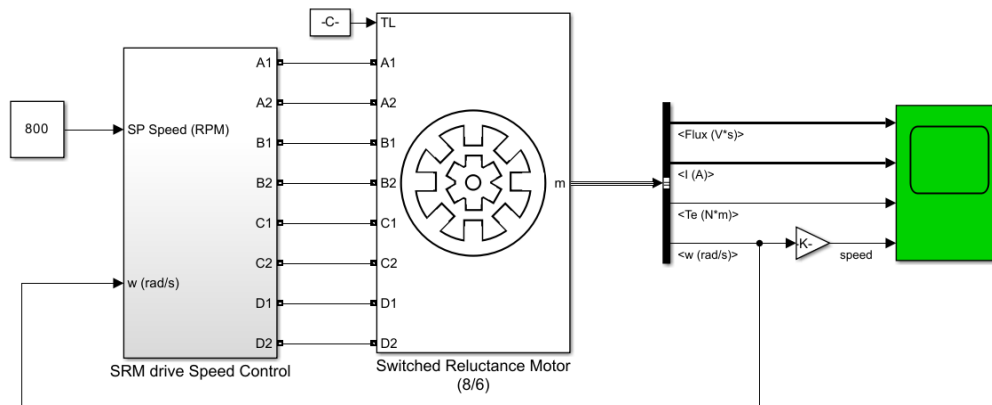

Figure 14. SRMs block diagram in MATLAB

Table 1. Parameters of SRM simulation

Description	Total
DC voltage	35 V
Switching control	PWM 10 kHz
Speed control	PI
Speed reference	800 rpm
Turn on angle	30º
Turn off angle	45º
Stator resistance	10 Ω
Load torque	0.04 N.m
Inertia constant	0.0005 kg.m^2
Viscous friction coefficient	0.005 N.m.s
Unaligned inductance	35 mH
Aligned inductance	150 mH
Maximum current	3 A
Current reference	2.7 A

Moving on to the simulation results, Figures 15-17 provide a comprehensive overview of the AHB, shared switch, and Miller topologies, respectively. Figure 16 illustrates the performance of the AHB converter. Figures 15(a)-15(b) show flux and current capture of the data at a specific time interval between 0.47 and 0.5 seconds. During steady-state operation, the AHB converter showed a maximum phase current of 0.67 A, with a switching period of 12.46 ms for each phase. Moreover, the average phase current for the AHB was recorded at 0.41 A. Figure 15(c) shows the torque electric rms in steady-state conditions at 0.04 N.m. Figure 15(d) shows that speed control is succeeding in reaching the setpoint at 800 rpm.

Figure 16 illustrates the performance of the Shared Switch converter. The simulation results showed that it has the same performance as the AHB Converter. Figures 16(a)-16(b) show flux and current capture of the data at a specific time interval between 0.47 and 0.5 seconds. During steady state operation, the Shared Switch converter showed a maximum phase current of 0.67 A, with a switching period of 12.46 ms for each phase. The average phase current for the Shared Switch was recorded at 0.41 A. Figure 16(c) shows the torque

electric rms in steady state condition is 0.04 N.m. Figure 16(d) shows that speed control is succeeding to reach the setpoint at 800 rpm.

However, Figure 17 shows the simulation result from Miller converter. Figures 17(a) and 17(b) show the flux and current. The current shows the overlap condition between each phase. This current waveform occurred because there is not enough time for each phase to demagnetize. As you can see in Figure 17(b), when phase A is demagnetizing, phase B is directly magnetizing. The switching period is 16.74 ms for each phase. Figure 17(c) shows the torque electric rms in steady state condition is 0.033 N.m, but Figure 17(d) shows that the speed of the SRM controlled by Miller converter cannot reach 800 rpm. The maximum speed is 599 rpm. For this reason, we need to change the parameter of the Miller topology for demagnetizing. We need to decrease the turn off angle of the Miller converter. The new parameter is explained in Table 2.

Table 2. New parameter for Miller converter

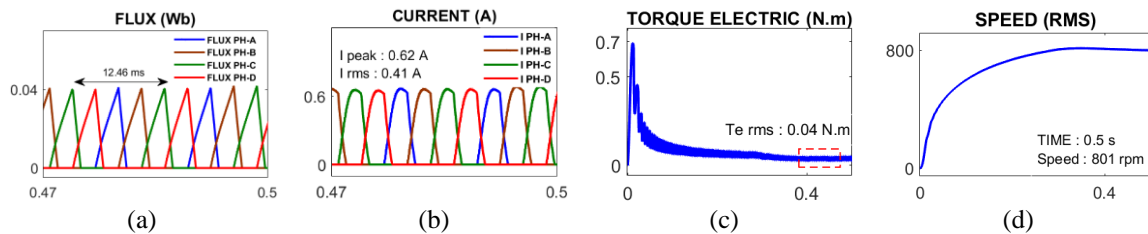| Description	Total
Speed reference	500 rpm
Turn On angle	30°
Turn Off angle	41°

Figure 15. AHB converter simulation results for (a) phases flux, (b) phases current, (c) torque electric, and (d) speed control
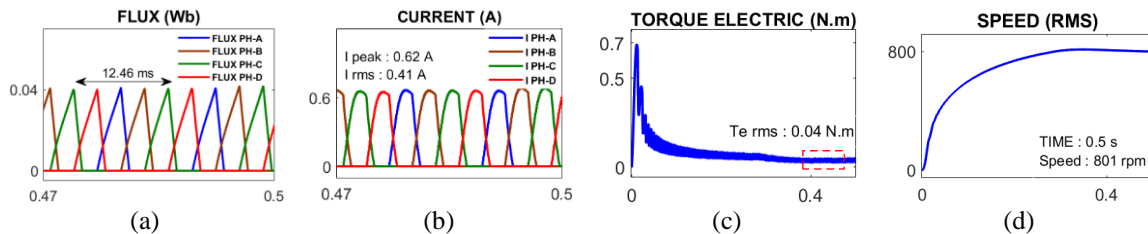

Figure 16. Shared Switch converter simulation results for (a) phases flux, (b) phases current, (c) torque electric, and (d) speed control
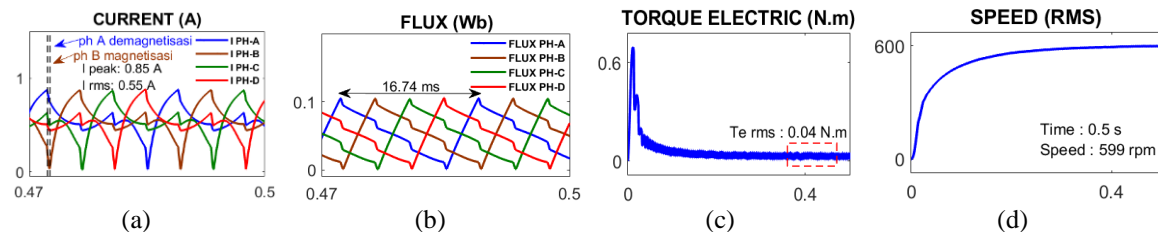

Figure 17. Miller converter simulation results for (a) phases flux, (b) phases current, (c) torque electric, and (d) speed control

The new simulation result for Miller converter is described in Figure 18. Figures 18(a) and b18(b) show the flux and current. From Figure 18(b), as we can see, the current does not show any overlapping condition, and each phase has time for de-magnetizing itself. The peak current shows 0.81 with the rms 0.28

A. With this current and voltage applied, the Miller converter still cannot reach 800 rpm. The parameter is mentioned as the speed reference becoming 500 rpm to find out the control modelling. Figure 18(c) shows the torque electric produced by the SRM, and it shows 0.03 N.m. The control can maintain the Miller converter at 500 rpm as described in Figure 18(d).
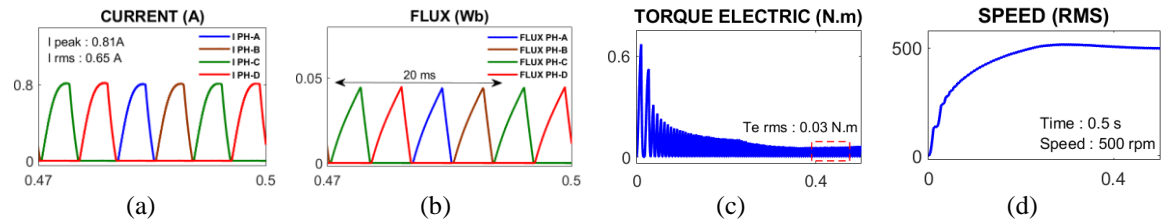

Figure 18. Miller converter with new parameters simulation results for (a) phases flux, (b) phases current, (c) torque electric, and (d) speed control

4.   EXPERIMENTAL RESULT

For the verification of the speed control modeling, we are using TMS320F2837D as a microcontroller to process the signal and determine the switching of the MOSFET. This device is programmed in MATLAB. Figure 19 shows the experiment setup. The experiments conducted involved the utilization of AHB, shared switches, and Miller converters. The switching frequency used to drive the MOSFET was set to 10 kHz, while a power supply of 35 Volts was connected to provide the necessary power to the motor. The experiment parameter and the SRM parameter are mentioned in Table 1. The SRMs motor is also loaded by generator DC to see the performance and actual speed of each topology.
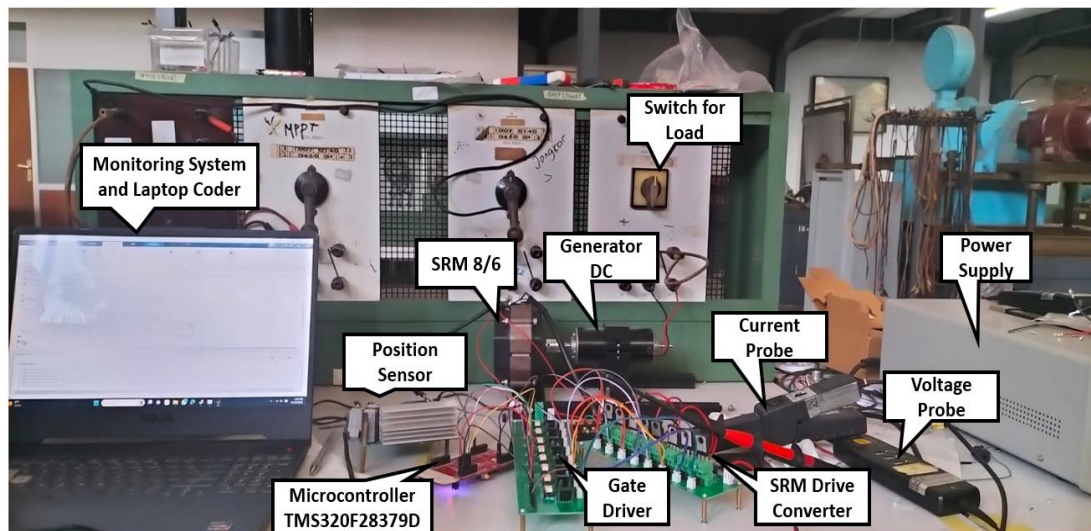

Figure 19. Experimental setup

Figure 20(a) shows phase voltage A, current A, speed control, and actual speed while loaded. As you can see, when the phase starts magnetizing, the current starts rising. The experiment shows that the peak current of the SRM is 0.63 A, while the simulation shows 0.62 A and the current waveform is slightly different between the simulation and the experiment. The difference between simulation and experiment happened because we did not model the characteristic of magnetization of the experiment, the SRM 8/6, in simulation. Since we are using the generic model in the simulation, the magnetization characteristics are different between the simulation and the experiment SRM 8/6. The speed control is working, as we can see from the set point speed (SP) and actual value (PV). When the 15 W loads are applied by closing the load switch, the control can maintain the speed at 800 rpm.

In Figure 20(b), the shared switch converter results also show the same performance as the AHB converter. The unique characteristics of a shared switch converter are sharing a switch for the adjacent phase, as shown on the phase voltage on La and Lc. The current through the switch S2 is showing the current for

phases A and C. The peak current and the waveform are equal with the AHB converter. The peak current is 0.63 A. The speed control is also working, as we can see from the set point speed (SP) and actual value (PV). When the 15 W loads are applied by closing the load switch, the control can maintain the speed at 800 rpm.

Figure 20(c) shows the experimental result of Miller topology. The commutation angle is already reduced (it has the same parameter as Table 2), and the voltage figures show that the phase voltage A and phase voltage B are not demagnetized and magnetized at the same time. There is a time for the phase to fully demagnetize until the current is zero, then continue to the next phase. S1 carries all the phase current since it is shared for all of the phases. When the motor is loaded with 15 W, the motor cannot maintain the speed at 800 rpm. With this condition, the maximum speed, the Miller converter can reach is 550 rpm. We change the set point to 500 rpm when loaded, and after that, we try to switch off the load, and the Miller converter can maintain the speed at 500 rpm.
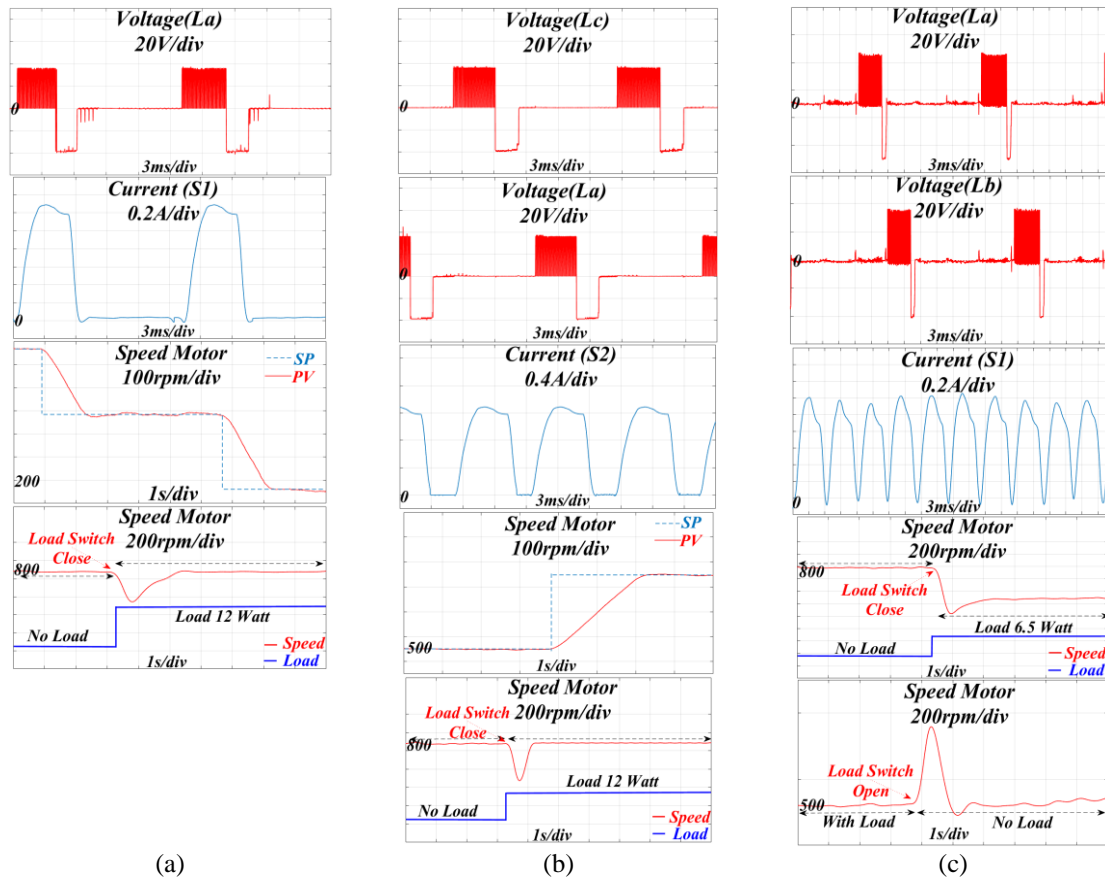

Figure 20. Phase voltage, phase current, changing setpoint of speed, and speed control motor with load for (a) AHB, (b) shared switch, and (c) Miller

5.   CONCLUSION

This research paper extensively examines the proposed control strategy for driving the SRM 8/6 by modelling the speed control in MATLAB/Simulink. The experiment using the TMS320F2837D device with function block logic in MATLAB/Simulink was also proposed in this research. The AHB, Shared Switch, and Miller converter are used and compared to prove the proposed control strategy. The simulation and experimental results show that the control model can drive and control the speed of the SRM with all types of converters. The performance in the experiment validates the simulation for all types of converters, The performance of the Shared switch shows equal with the AHB converter. Interestingly, the Shared Switch converter only consists of six switches and six diodes. which are less than AHB. The Miller converter shows the fewest components needed by only consisting of five switches and five diodes, but the performance of the Miller converter is not better than the other topologies. To summarize, the shared switch converter offers a preferable solution for driving the SRM with an even number of phases. This preference is primarily due to its cost-effectiveness, as it requires fewer components.

REFERENCES

[1] R. Jarvis, "Davidson's locomotive: How did he do it?", *Engineering Science and Education Journal*, vol. 5, no. 6, pp. 281-288, Dec. 1996, doi: 10.1049/esej:19960613.

[2] T.J.E. Miller , *Electronic Control of Switched Reluctance Machines*. Elsevier, 2001.

[3] S. Singh, S. Singh, and G. Bhuvaneswari, "Comparison of converter control strategies for a switched reluctance machine," in *2022 IEEE Delhi Section Conference (DELCON)*, New Delhi, 2022, pp. 1-5, doi: 10.1109/icems.2017.8056533.

[4] Y. Hu, C. Gan, Q. Sun, P. Li, J. Wu, and H. Wen, "Modular tri-port high-power converter for SRM based plug-in hybrid electrical trucks," *IEEE Transactions on Power Electronics*, vol. 33, no. 4, pp. 3247-3257, April 2018, doi: 10.1109/tpel.2017.2701784.

[5] E. Zhao, S. Song, Z. Ma, X. Zhang, L. Ning, and Y. Liu, "Design and initial testing of an integrated switched reluctance starter/generator system for unmanned aerial vehicle," *CES Transactions on Electrical Machines and Systems*, vol. 2, no. 4, pp. 377-383, Dec. 2018, doi:10.1109/access.2020.2986393.

[6] I. Ralev, F. Qi, B. Burkhart, A. Klein-Hessling, and R. W. De Doncker, "Impact of smooth torque control on the efficiency of a high-speed automotive switched reluctance drive," *IEEE Transactions on Industry Applications*, vol. 53, no. 6, pp. 5509-5517, Dec. 2017, doi: 10.1109/tia.2017.2743680.

[7] T. Husain, A. Elrayyah, Y. Sozer, and I. Husain, "Unified control for switched reluctance motors for wide speed operation," *IEEE Transactions on Industrial Electronics*, vol. 66, no. 5, pp. 3401-3411, May 2019, doi: 10.1109/tie.2018.2849993.

[8] R. Krishnan, *Switched Reluctance Motor Drives -. Simulation, Analysis, Design, and Applications*. London: CRC Press, 2001, doi: 10.1201/9781420041644.

[9] J. Furqani, C. A. Wiguna, A. Chiba, O. Gundogmus, Y. Sozer, and A. Purwadi, "Experimental verification of acoustic noise and radial force sum variation in switched reluctance motor," *IEEE Transactions on Industry Applications*, vol. 57, no.3, pp. 2481–2493, March 2021, doi: 10.1109/tia.2021.3066955.

[10] C. A. Wiguna, J. Furqani, and A. Chiba, "Improved current profile selection for noise reduction of switched reluctance motor at middle speed considering back EMF," *IEEE Transactions on Industry Applications*, vol. 57, no.5, pp. 4707-4719, Sep. 2021, doi: 10.1109/tia.2021.3091085.

[11] D. E. Cameron, J. H. Lang and S. D. Umans, "The origin and reduction of acoustic noise in doubly salient variable-reluctance motors," in *IEEE Transactions on Industry Applications*, vol. 28, no. 6, pp. 1250-1255, Nov.-Dec. 1992, doi: 10.1109/28.175275.

[12] W. Cai, P. Pillay, Z. Tang and A. M. Omekanda, "Low-vibration design of switched reluctance motors for automotive applications using modal analysis," in *IEEE Transactions on Industry Applications*, vol. 39, no. 4, pp. 971-977, 2003, doi: 10.1109/TIA.2003.814559.

[13] R. S. Colby, F. Mottier and T. J. E. Miller, "Vibration modes and acoustic noise in a 4-phase switched reluctance motor," IAS '95. *Conference Record of the 1995 IEEE Industry Applications Conference Thirtieth IAS Annual Meeting*, Orlando, FL, USA, 1995, pp. 441-447 vol.1, doi: 10.1109/IAS.1995.530333.

[14] B. P. Reddy, R. V. Janaki, and K. S. Kumar, "Torque ripple minimization of SRM using sense coils and FPGA," in *2020 IEEE International Conference on Power Electronics, Smart Grid and Renewable Energy (PESGRE2020)*, Cochin, India, 2020, pp. 1-6, doi: 10.1109/pesgre45664.2020.9070690.

[15] C. Gan, J. Wu, Q. Sun, W. Kong, H. Li, and Y. Hu, "A review on machine topologies and control techniques for low-noise switched reluctance motors in electric vehicle applications," *IEEE Access*, vol. 6, pp. 31430-31443, 2018, doi: 10.1109/access.2018.2837111.

[16] J. Castro, P. Andrada, and B. Blanqué, "Minimization of torque ripple in switched reluctance motor drives using an enhanced direct instantaneous torque control," in *2012 XXth International Conference on Electrical Machines*, Marseille, France, 2012, pp. 1021-1026, doi: 10.1109/icelmach.2012.6350001.

[17] X. Cui, J. Sun, C. Gan, C. Gu, and Z. Zhang, "Optimal design of saturated switched reluctance machine for low speed electric vehicles by subset quasi-orthogonal algorithm," *IEEE Access*, vol. 7, pp. 101086-101095, 2019, doi: 10.1109/access.2019.2929103.

[18] R. Martua, J. Furqani, and A. Rizqiawan, "Performance comparison of the 8/6 SRM inverters," in *2022 5th International Conference on Power Engineering and Renewable Energy (ICPERE)*, 2022, vol. 1, pp. 1-6, doi: 10.1109/icpere56870.2022.10037316.

[19] E.S. Elwakil and M.K. Darwish, "Critical review of converter topologies for switched reluctance motor drives," *International Review of Electrical Engineering*, vol. 2, no. 1, Jan. 2011.

[20] C. Pollock and A. Michaelides, "Switched reluctance drives: a comparative evaluation," *Power Engineering Journal*, vol. 9, no. 6, pp. 257-266, Dec. 1995, doi: 10.1049/pe:19950606.

[21] M.R. Harris, J.W. Finch, J.A. Mallick, and T.J.E. Miller, "A review of the integral-horsepower switched reluctance drive," *IEEE Transactions on Industry Applications*, vol. IA-22, no. 4, pp. 716-721, Jul. 1986, doi: 10.1109/tia.1986.4504783.

[22] M. F. S. Pereira, A. Mamede, and R. Esteves Araújo, "Switched reluctance motor drives: fundamental control methods," in *Modelling and Control of Switched Reluctance Machines*. IntechOpen, Sep. 09, 2020, doi:10.5772/intechopen.90476.

[23] M. Hamouda and L. Szamel, "A new technique for optimum excitation of switched reluctance motor drives over a wide speed range," *Turkish Journal of Electrical Engineering and computer sciences*, vol. 26, no. 5, pp. 2753–2767, 2018, doi: 10.3906/elk-1712-153

[24] Z. Zhang, N.C. Cheung, K.W.E. Cheng, X.D. Xue, J.K. Lin, and Y.J. Bao, "Analysis and design of a cost-effective converter for switched reluctance motor drives using component sharing," in *2011 4th International Conference on Power Electronics Systems and Applications*, Hongkong, 2011, pp. 1-6, doi: 10.1109/pesa.2011.5982962.

[25] S. Vukosovic and V. R. Stefanovic, "SRM inverter topologies: A comparative evaluation," *IEEE Transactions on Industry Applications*, vol. 27, no. 6, pp. 1034-1047, Nov. 1991, doi: 10.1109/28.108453.

BIOGRAPHIES OF AUTHORS

Ronaldo Martua 🆔 📇 ᔆᶜ ◯ was born in Bandung, Indonesia in 1993. He graduated and received a bachelor's degree from the Institut Teknologi Bandung, Indonesia in 2015. Now he is currently pursuing his master's degree in Electrical Engineering at Institut Teknologi Bandung. He is interested in research about power electronics and switched reluctance motor drives. He can be contacted at email: ronaldomartua@gmail.com.

Alam Raihan Emir ⓘ 🅖 SC ◑ was born in Ipoh, Malaysia. He graduated and received the bachelor's degrees from the Institut Teknologi Bandung, Indonesia in 2024. His main research is in power electronics, electrical machines, and motor drives. He was a research assistant at JFRG team and was a laboratory assistant for electric machinery and electric power lab. He can be contacted at email: alamraihan.emir@gmail.com.

Michael Suhendra ⓘ 🅖 SC ◑ was born in Jakarta. He graduated and received the bachelor's degrees from the Institut Teknologi Bandung, Indonesia in 2024. His main research, with other members on the team, is in power electronics, especially in SRM (switched reluctance motor) inverter shared switch topology. He was a research assistant at JFRG team and was a laboratory assistant for electric machinery and electric power lab. He can be contacted at email: michaelsuhendra22@gmail.com.

Denri Yesayevtta ⓘ 🅖 SC ◑ graduated and received the bachelor's degrees from the Institut Teknologi Bandung, Indonesia in 2023. He was a research assistant of JFRG for this project. The research includes power converter as electric motor controller. He also was a teaching assistant for electric machinery and electric power practicum at Electrical Energy Conversion Research Laboratory ITB. He can be contacted at email: sihalohodenri@gmail.com.

Arwindra Rizqiawan ⓘ 🅖 SC ◑ received the bachelor's and master's degrees from the Insititut Teknologi Bandung, Bandung, Indonesia, in 2006 and 2008, respectively, and a doctoral degree from the Shibaura Institute of Technology, Tokyo, Japan, in 2012, all in Electrical Engineering. He is currently serving as an Assistant Professor with the School of Electrical Engineering and Informatics, Institut Teknologi Bandung. He is currently a Certified Professional Engineer in Indonesia with the Institution of Engineers Indonesia and ASEAN Engineer by ASEAN Engineering Register. His research interests include power engineering, power electronics, and renewable energy. He can be contacted at email: windra@itb.ac.id.

Jihad Furqani ⓘ 🅖 SC ◑ was born in Malang, East Java, Indonesia in 1990. He received B.S. degree in Electrical Power Engineering from Bandung Institute of Technology in 2012. He received an M.S. degree in Electrical Engineering from Bandung Institute of Technology in 2013. He received a Doctor of Engineering degree in Electrical and Electronic Engineering from the Tokyo Institute of Technology in 2019. He has been studying multilevel and multiphase motor drive, noise reduction in switched reluctance motor, power electronic converter for renewable energy application, electric motor for vehicle application, and electric machine in power system. He was a visiting researcher of University of Akron in 2017 and visiting lecture of Tokyo Institute of Technology in 2021. He was research assistant professor in Electrical Power Engineering, School of Electrical Engineering and Informatics, National Center for Sustainable Transportation Technology, and Center for Instrument Technology and Automation, Bandung Institute of Technology. Currently, He is Head of Drivetrain System in MAKA-Motors. He is Certified Professional Engineer in Indonesia, ASEAN, and Asia Pacific. He received IEEE Star Reviewer in 2019 and IEEE Indonesia Section Recognition in 2022. He can be contacted at email: j.furqani@yahoo.com.